Deterministic assembly of channeling cracks as a tool for nanofabrication

2010 Nanotechnology 21 055301

(http://iopscience.iop.org/0957-4484/21/5/055301)

Nanotechnology **21** (2010) 055301 (10pp) doi:10.1088/0957-4484/21/5/055301

Deterministic assembly of channeling cracks as a tool for nanofabrication

B Erdem Alaca[1], Can Ozcan[2,3] and Gunay Anlas[2]

[1] Department of Mechanical Engineering, Koc University, Rumeli Feneri Yolu, 34450 Sariyer, Istanbul, Turkey
[2] Department of Mechanical Engineering, Bogazici University, 34342 Bebek, Istanbul, Turkey

E-mail: ealaca@ku.edu.tr

Received 18 October 2009, in final form 2 December 2009
Published 24 December 2009
Online at stacks.iop.org/Nano/21/055301

Abstract
To address the necessity for a predictive computational tool for layout design in crack lithography, a tool for nanowire fabrication, a computational study is carried out using finite element analysis, where crack-free edge and crack–crack interactions are studied for various material combinations. While the first scenario addresses the ability to induce a controlled curvature in a nanowire, the latter provides an estimation of the minimum distance which can be kept between two straight nanowires. The computational study is accompanied by an experimental demonstration on Si/SiO_2 multilayers. Finite element results are found to be well aligned with experimental observations and theoretical predictions. Stronger interaction is evident with a curved crack front modeling as well as with increasing first and decreasing second Dundurs' parameters. Therefore cracks can be packed closer with decreasing film stiffness.

(Some figures in this article are in colour only in the electronic version)

1. Introduction

Cracks encountered in thin film/substrate systems exhibit a variety of patterns. Of special interest are channeling cracks that propagate in the thin film until they meet another crack or a free edge [1]. A cracking pattern results out of this collective behavior of multiple cracks. The nature of such cracking and resulting patterns are due to a complex interdependence among the nature of loading [2], substrate anisotropy [3], crack interactions [4], elastic mismatch between thin film and substrate as well as interfacial strength [5, 6]. It is also well known that stress raisers in multilayers, such as integrated circuit structures, serve as crack initiators and hence affect the resulting fracture pattern [7]. Various numerical studies on the evolution of crack patterns as a result of such initial distribution of defects/stress raisers are reported in the literature [8, 9].

The observation of the effect of stress raisers on crack formation led to the idea of controlling crack patterns by imposing a known stress field in a thin film coated on a substrate [10]. If cracks in the thin film arrest at the interface, they can further be utilized as molds to be filled with a second material, leading to nanowire (NW) formation as depicted in figure 1(a). The initial demonstration of this idea was carried out on a Si/SiO_2 substrate/thin film system, where stress-raising features (sharp corners in figure 1(b)) were etched in the Si substrate. After deposition of a 5 μm thick SiO_2 film by plasma-enhanced chemical vapor deposition (PECVD), the system was subjected to thermal loading, where a condensation reaction took place in an SiO_2 film, turning the initially compressive film stress into tensile [11]. Following the formation of tensile stresses, cracks were observed to initiate specifically at sharp corners as shown in figure 1(b). Furthermore, free edges, again etched in Si, were utilized as crack attraction sites, where cracks terminate. This initial study was followed by further work on the explanation of the mechanism of tensile stress generation and crack formation as a function of the nature of the deposition process and the chemistry of the specific Si/SiO_2 system [12, 13]. Removal of the cracked layer after the filling process is complete would provide a negative replica of the crack network made of NWs (figure 1(c)). Electroless deposition [10] and electrodeposition [14] were the techniques of choice for obtaining Ni and NiFe NWs, respectively.

Alternatives to Si/SiO_2 system were proposed by the Adelung group. Reaching sub-10 nm NWs was possible with

[3] Present address: Ozen Engineering, Incorporated, 1210 East Arques Avenue, Sunnyvale, CA 94085, USA.

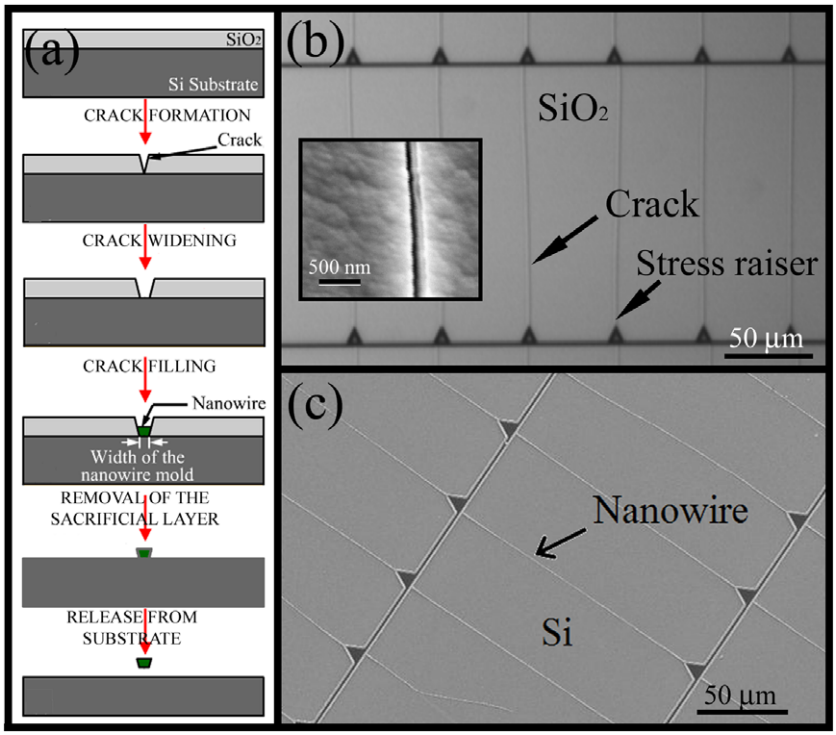

Figure 1. (a) Fabrication sequence of NWs. (b) Cracks obtained in the SiO_2 coating with the inset showing a detailed top view of a single crack. It is observed that maximum crack opening is obtained at the free surface, whereas it decreases toward the interface. (c) NWs obtained by filling the cracks in (b).

the crack technique as demonstrated with Teflon-AF films on graphite [15]. Other thin film/substrate systems, where cracking without deterministic assembly was demonstrated, include photoresist thin films (POSITIV 20) on stainless steel or polymer foils, poly(methyl methacrylate) on silicon, amorphous carbon thin film on glass or Nafion® substrates, amorphous fluoropolymeric thin film on polyimide or graphite substrates [15, 16]. Patterning was also demonstrated using photoresist thin films on Si [17].

The achieved level of NW assembly is capable of meeting the requirements of technology development for the integration with microelectromechanical systems (MEMS). Figure 2 depicts the utilized approach. In the first layer one defines sharp corners and free edges, initiation and termination locations of NWs, respectively. The second layer constitutes microscale components. Finally, NWs are to be disconnected from termination sites and released from the substrate. The approach was demonstrated in the case of a microgripper, where the level of integration was far more complex than a simple electrode–NW attachment problem [18]. In fact, the technique is comparable to other self-assembly-based patterning techniques for NWs, where, instead of mechanical stress fields, electric, magnetic or fluidic flow fields are utilized to assemble NWs (references in [14]). Similar to these cases where a prior knowledge of the distribution of the field strength is instrumental in designing the microsystem, knowledge on the distribution of stresses in a given layout is necessary for a successful implementation of the crack technique. This raises the need for detailed simulations of crack propagation.

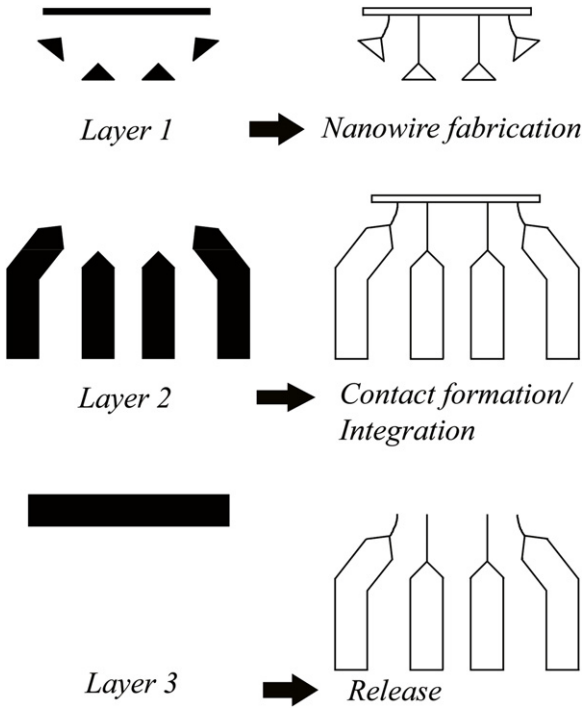

Figure 2. The approach to monolithic micro–nano integration using crack patterning.

A variety of modeling approaches for crack propagation are adopted in the literature. Among analytical treatments of the problem, one can mention the work by Thouless [19],

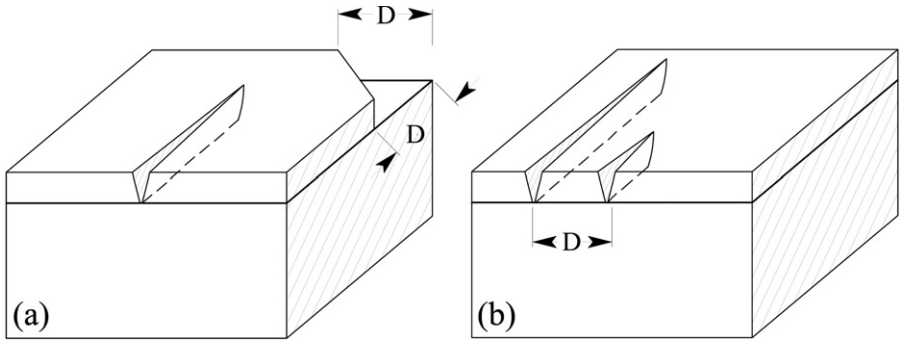

Figure 3. Two geometries considered in this work. (a) A single crack interacting with a free edge. (b) A single crack interacting with a neighboring crack.

where minimum spacing between parallel cracks in a brittle film was calculated as a function of applied stress and fracture toughness of the thin film. Xia and Hutchinson [4] adopted a numerical scheme utilizing an elastic restoring force with a given spring constant to account for the substrate effect and dislocation doublets to model channeling cracks. An alternative approach was recently developed by Yin *et al* [20], where a section between two cracks in a thin film/substrate structure with periodic cracking was treated as a representative element with periodic boundary conditions to attain a closed form solution for the displacement field.

For the prediction of exact crack propagation paths, finite element analysis is unmatched in its range of capabilities and remains as one of the most preferred computational tools. Liang *et al* [8] used a shear lag model along with an extended finite element analysis. Details on computing the associated energy release rate can be found in [21]. Recently, Liu and Chen [22] employed the same approach to estimate the crack attraction capability of voids embedded in thin films.

In this work, a similar finite element modeling with remeshing is used for a parametric study of two cases as depicted in figure 3.

Case 1. A single crack channeling in the thin film toward a slanted free edge. This set-up is necessary for imparting a controlled curvature to the crack path. When approaching the free edge, the crack is expected to divert from its straight path and meet the free edge. This geometry is expected to result in a single NW with a predetermined curvature, a structure that is very difficult to obtain with other self-assembly-based techniques.

Case 2. Two parallel cracks channeling in the thin film. There is a neighborhood of reduced stresses around a crack, whose size is characterized by the decay length as described by Xia and Hutchinson [4]. If another crack is brought into this zone, it will be attracted toward the existing crack, thereby diverting from its straight path. On the other hand, if a sharp corner is etched in this zone, a crack might not initiate at all due to insufficient energy stored in the material. Hence, this particular set-up is important for predicting the minimum permissible distance between two straight NWs.

In addition, experimental observations with specifically designed layouts in an Si/SiO_2 system are also provided for both cases. These observations do not only serve as a motivation for further computational work, but they also indicate the potential of the aforementioned technique for the batch-compatible integration of micro- and nanoscale objects. In the remainder of this work, both experimental observations and finite element simulations for the two configurations will be discussed. Comparison with theory available in literature will be provided.

2. Crack-free edge interactions

2.1. Experimental observations

To study the crack-free edge interactions, a set of samples were fabricated using the aforementioned oxide deposition technique. Si in the form of 4 inch diameter, n-doped ⟨100⟩ wafers with a thickness of 450–575 μm was used as the substrate material. Two features were etched in the Si substrate: a sharp crack initiator and a slanted free edge. The distance between the crack initiator and the free edge was changed in a systematic manner by moving the free edge toward the crack initiator. Etching of these features was followed by the deposition of the oxide coating. Associated process parameters can be found in [10]. In the micrographs of figure 4, the oxide coating is shown in the form of a 330 μm $\times$ 330 μm square with a cut corner (lower right corner) serving as the free edge. The shiny Si surface is visible at the bottom of the free edge and the initiator. Upon exposure to thermal loads, cracks were observed to form and they were subsequently attracted to the free edge. The micrographs show that the approaching crack continuously adjusts its path by maximizing the opening stress. On the free edge, tractions vanish and stress parallel to the free edge becomes the maximum stress component. Hence, the crack was expected to meet and arrest at the free edge with ninety degrees, perpendicular to the maximum in-plane stress.

2.2. Computational modeling

Similar to other crack interaction studies in the literature [8], the maximum tangential stress (MTS) criterion [23] was used for the study of crack propagation. The criterion can be applied to brittle materials under slowly applied plane loads and is based on the hypothesis that crack propagation takes place

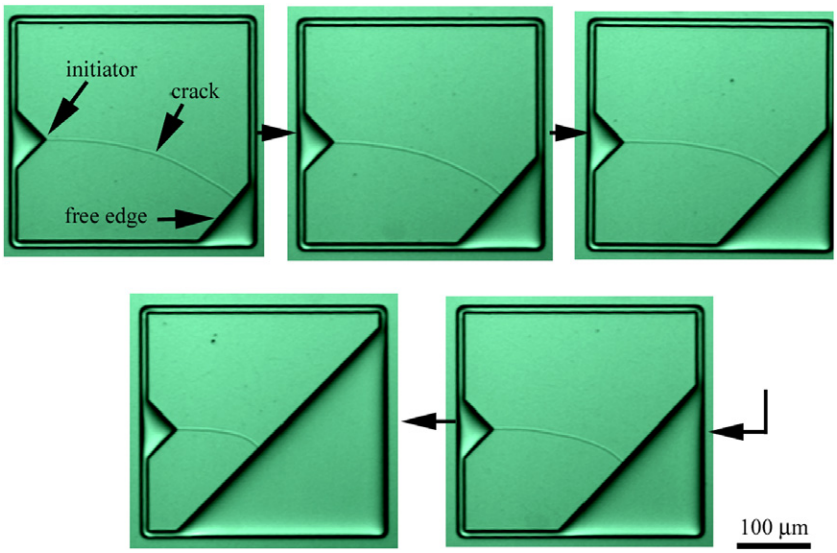

Figure 4. Micrographs showing the effect of a slanted free edge on the path of an approaching crack. The observation is based on the systematic variation of the relative location of the free edge with respect to a crack initiator.

along the direction perpendicular to the maximum tangential stress, $\sigma_{\theta\theta}$, around the crack tip. Therefore, tangential stresses at the nearest nodes on a circle centered around the crack tip were calculated and the maximum tangential stress was determined.

This quasi-static crack propagation study was carried out using ANSYS on the geometry shown in figure 3(a) [24]. A finite element model, consisting of quadratic tetrahedral and hexahedral elements for the elastic substrate and the thin film, respectively, was built using linear elastic material models. To introduce singularity, the crack tip region was meshed with 1/4 skewed midside-noded elements. A structural grid with an element at every 30° was built around the crack tip to capture near-tip displacements accurately. This planar mesh was then extruded along the film thickness direction with 10 separate layers to achieve a three-dimensional crack front representation. An arc-shaped crack front was also considered through the analysis by means of employing a specific crack front node shifting algorithm as explained later.

The interface between the thin film and the substrate was modeled as perfectly bonded by using coincident nodes. Film thickness, h (5 μm), was taken as 1/80 th of the substrate thickness throughout the analysis. A region of 300 μm $\times$ 300 μm was considered. During the analysis the whole structure was loaded with thermal body forces by exposing it to a temperature drop. This is a method of fictitious stress generation. Actual substrate–thin film systems might exhibit film shrinkage [10] or substrate swelling [15] due to reasons other than the mismatch of coefficients of thermal expansion. Considering the experimental set-up of the problem, symmetry boundary conditions were applied at four vertical faces of the unit cell.

The materials mismatch between the thin film and the substrate was modeled by considering Dundurs' mismatch parameter α:

$$\alpha = \frac{E_f/(1-\nu_f^2) - E_s/(1-\nu_s^2)}{E_f/(1-\nu_f^2) + E_s/(1-\nu_s^2)} \tag{1}$$

with E_f and E_s representing the elastic moduli of the thin film and the substrate, respectively [25]. Similarly, ν_f and ν_s indicate Poisson's ratios of the thin film and the substrate, respectively. In the case of a stiff substrate and a relatively compliant thin film with similar Poisson's ratios, α becomes negative. In the limit, when the substrate becomes rigid, α assumes the value of -1. For the cases under consideration, the second Dundurs' parameter [25], β in equation (2), is taken as $\alpha/4$ and $3\alpha/8$, where G_f and G_s are the shear moduli of the thin film and the substrate, respectively:

$$\beta = \frac{G_f(1-2\nu_s) - G_s(1-2\nu_f)}{2G_f(1-\nu_s) + 2G_s(1-\nu_f)}. \tag{2}$$

It is to be noted that in regard to the experimental study of PECVD SiO_2 on a ⟨100⟩ Si substrate, it is difficult to come up with a single pair of Dundurs' parameters due to the substrate's anisotropy. It is well known that $E_s/(1-\nu_s) = 180.5$ GPa is invariant within the plane of the substrate, with E_s taking the extreme theoretical values of 168.9 GPa ($\nu_s = 0.064$) along ⟨011⟩ and 103.2 GPa ($\nu_s = 0.428$) along ⟨100⟩ [26]. Similarly, in the literature, one can find $E_f \approx 75$ GPa for silane-based PECVD oxides [27] and $\nu_f = 0.16$ for thermal oxide [28]. Mismatch parameters under the aforementioned conditions can then be roughly calculated as $\alpha = -0.376$ ($\beta = \alpha/2.8$) and $\alpha = -0.243$ ($\beta = \alpha/1.2$) along the ⟨011⟩ and ⟨100⟩ directions in Si, respectively. Therefore, rather than seeking a one-to-one correspondence between the simulations and the experimental observations, crack propagation as a function of geometry and materials mismatch will be studied.

Figure 5 shows the model of a thin film–substrate system with a slanted edge. For a mesh convergence study, five

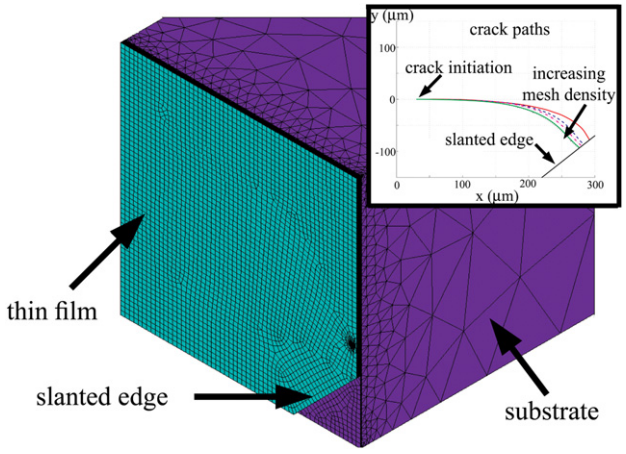

Figure 5. Finite element mesh for the crack-free edge interaction problem. The inset shows convergence of the associated crack propagation path with increased mesh density.

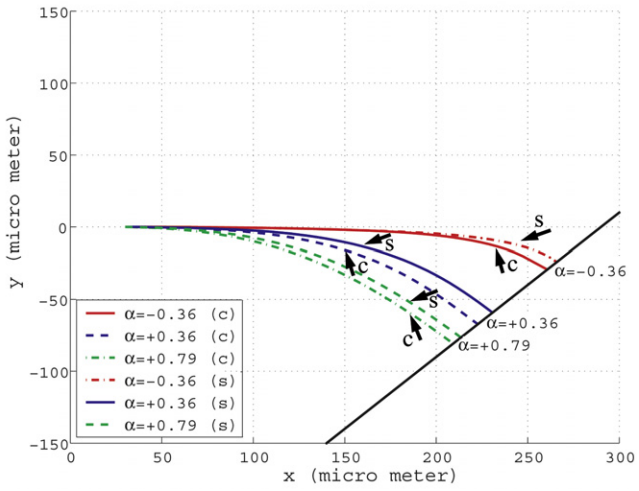

Figure 6. The effect of crack front shape. The use of a curved crack front (designated by c) is observed to lead to a higher amount of crack bending as opposed to the simulations utilizing a straight crack front (designated by s).

different mesh densities were used with this geometry. A mismatch of $\alpha = 0.79$ and $\beta = \alpha/4$ was chosen. The specific mesh in this figure has a total of 600 000 degrees of freedom. The inset summarizes the results. In all cases, the crack emanates from a single point and propagates toward the slanted edge. Beyond 600 000 degrees of freedom, no appreciable change in the crack path was observed. Hence, the rest of the computational study was carried out with this particular mesh density.

Prior to considering specific cases, the issue of crack front shape should also be addressed. As mentioned above, the computational model was not a two-dimensional one. Thus the shape of the crack front in the depth (thickness) direction was also investigated. Nakamura and Kamath [29] studied the three-dimensional steady-state crack front shape for rigid substrate and brittle thin film systems where, at steady state, the crack front was shown to attain a nearly parabolic shape once the crack length was approximately twice the film thickness. Under these conditions a nearly constant energy release rate distribution was obtained along the crack front.

Based on the Nakamura and Kamath [29] study, one can numerically determine the crack front shape using an iterative remeshing method such that a constant energy release rate is obtained along the crack front. The method includes remeshing where crack front nodes are shifted along the crack direction based on the difference between the plane strain energy release rate, G, calculated at a node and the average plane strain energy release rate, G_{av}, for the entire crack front. For example, if the energy release rate at a node is higher than the average value, then the node is shifted along the crack direction by an amount proportional to the normalized difference $(G - G_{\mathrm{av}})/G_{\mathrm{av}}$. This process was carried out for all crack front nodes and is repeated for several iterations. The steady-state crack front obtained as a result of this iterative analysis was used in the subsequent crack propagation analysis.

The crack propagation analyses of the inset in figure 5 were carried out using a straight crack front shape. To evaluate the effect of crack front geometry, a comparative study was carried out using straight and curved crack fronts for the geometry shown in figure 3(a) with $D = 160$ μm. Results given in figure 6 revealed minor differences, where cracks modeled with a curved front shape consistently bent earlier toward the slanted free edge, indicating a stronger interaction. Due to the consistency of this trend, straight crack front assumption was employed throughout the rest of this study.

Table 1. List of cases considered for simulations.

Case number	D (μm)	α	β
1	80	−0.36	$\alpha/4$
2	80	0.36	$\alpha/4$
3	80	0.79	$\alpha/4$
4	160	−0.36	$\alpha/4$
5	160	0.36	$\alpha/4$
6	160	0.79	$\alpha/4$
7	280	−0.36	$\alpha/4$
8	280	0.36	$\alpha/4$
9	280	0.79	$\alpha/4$
10	80	0.36	$3\alpha/8$
11	160	0.36	$3\alpha/8$
12	280	0.36	$3\alpha/8$
13	80	−0.36	$3\alpha/8$
14	160	−0.36	$3\alpha/8$
15	280	−0.36	$3\alpha/8$

For the main study, three different geometries were analyzed with a varying distance between the crack initiator and the free edge. Three cases with $\alpha = -0.36$, 0.36 and 0.79 were considered. Table 1 summarizes all cases analyzed for crack-free edge interaction studies. Parameter D in the table corresponds to the dimension defined in figure 3(a).

Resulting crack paths are given in figure 7. They show the prominent effect of α on the level of interactions. The distance between the crack initiation point and the free edge was at its maximum in figure 7(a), where no interaction was observed for $\alpha = -0.36$. However, with increasing α, the amount of interaction increased for the same geometry, which was evident from the fact that the deviation of the crack from its straight path occurred earlier. In figure 7(b), the free edge

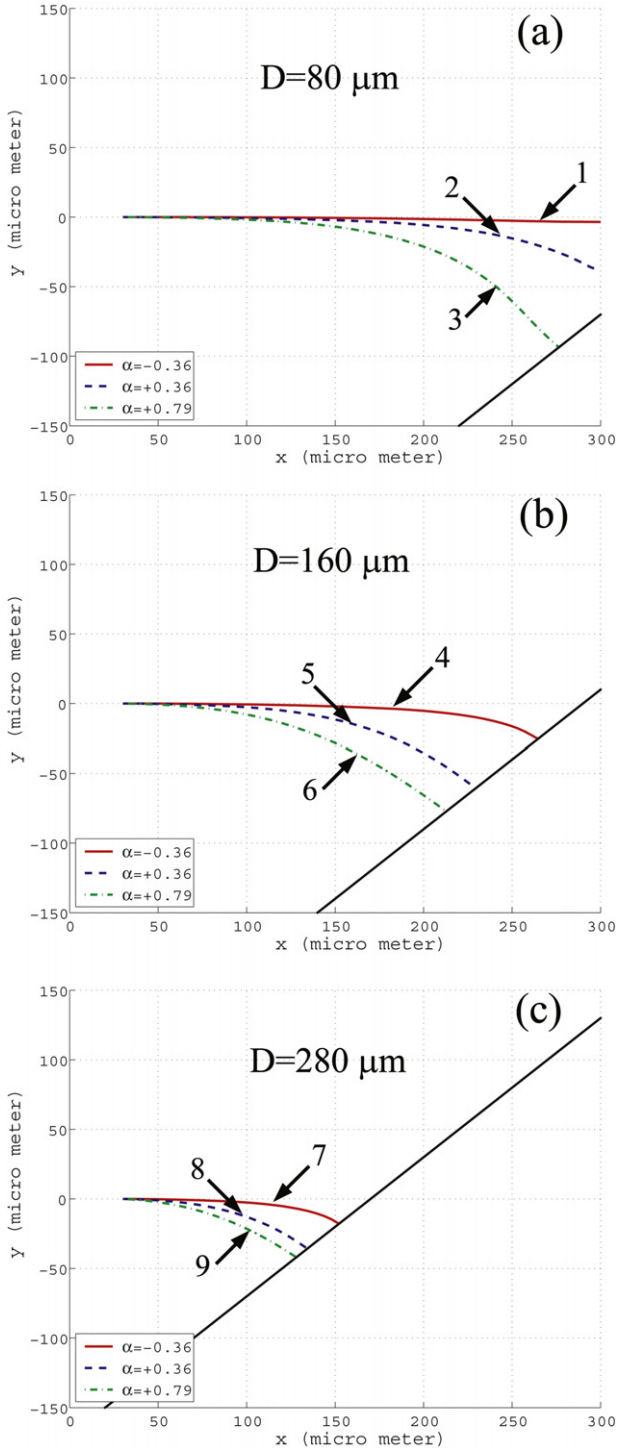

Figure 7. The interaction of a channeling crack with a slanted free edge for $\alpha = -0.36$, 0.36 and 0.79. It was observed that, with increasing α, the extent of the stress disturbance around the free edge increases, leading to a stronger interaction. Case numbers from table 1 are included on the plots. ($\beta = \alpha/4$.)

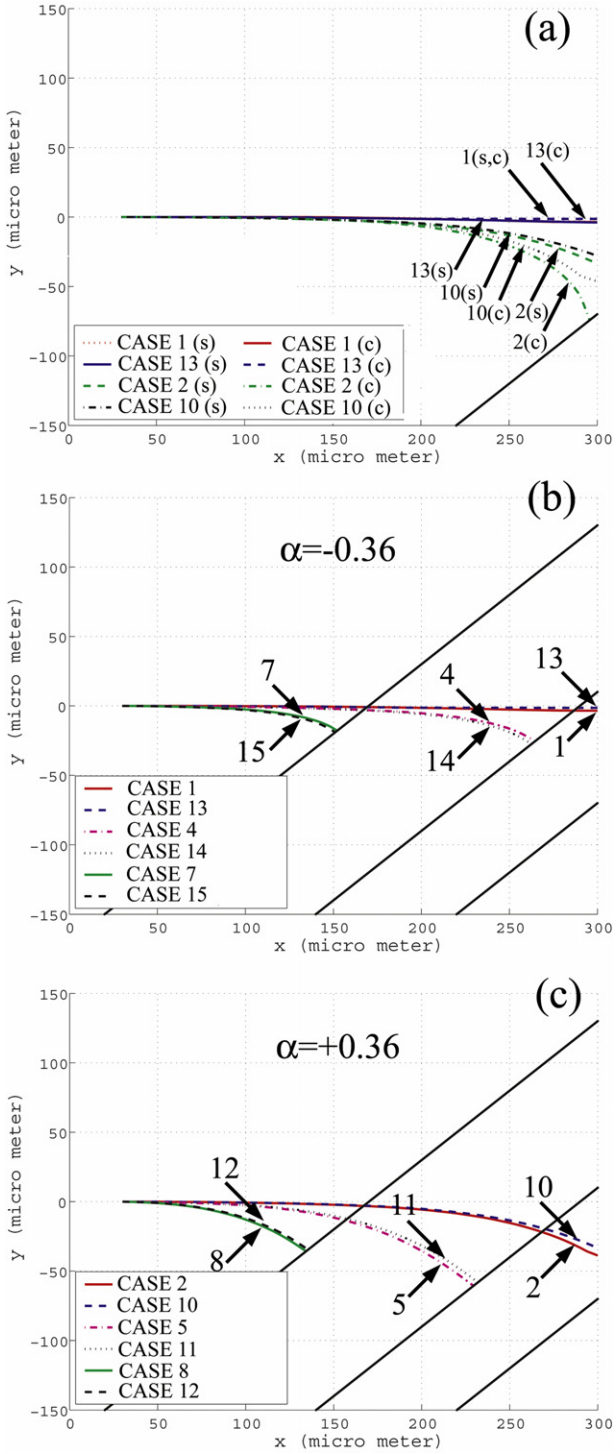

Figure 8. Effect of Dundurs' parameter β on the interaction of a channeling crack with a slanted free edge. Comparisons of cases with different β values shows a higher interaction with lower β, an effect that does not change with changing α. 's' and 'c' in (a) refer to straight and curved crack fronts, respectively.

was brought closer to the crack initiation point, leading to a diversion of the crack for all mismatch parameters. This behavior was repeated in a self-similar manner in figure 7(c), where a minimum distance was left between the initiation point and the free edge.

Similarly, the effect of β was studied and the results are given in figure 8 for different cases listed in table 1. The plot in figure 8(a) shows a comparison of two different α values, each calculated for two different values of β. A stronger interaction with lower β was observed for all α values studied. The effect

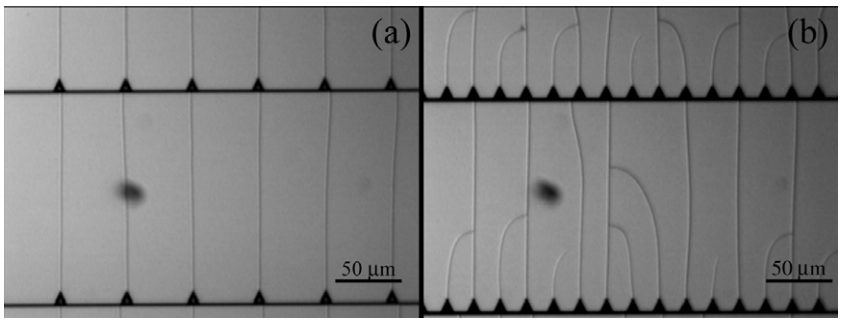

Figure 9. Micrographs of two configurations utilized for the experimental observation of crack–crack interactions. For the specific thin film/substrate system utilized in this work, no interaction was observed when neighboring cracks were placed 50 μm apart from each other, whereas a reduction of the crack spacing down to 20 μm resulted in an interaction manifested by the diversion of crack paths.

of the use of the curved crack front was once again evident in the form of stronger bending of the crack path. Hence, it was consistently shown that including the curved crack front shape in the modeling did not change the overall trend in crack paths. For example, in Case 2, the crack was still attracted stronger than it was in Case 10. However, the magnitude of this difference was amplified in the presence of the curved crack front.

Simulations of figures 8(b) and (c) were carried out with a straight crack front with different values of D as indicated by three separate slanted edges in each plot. The same trend, i.e. increasing interaction with lower β, was again indicated by these plots. It should be emphasized that a direct comparison of these results with experimental observations given in figure 4 would not be possible without a proper treatment of the substrate anisotropy.

The geometry of the problem provides a controlled way of diverting a straight crack from its propagation direction. This leads to the possibility of imposing a predetermined curvature to the NW, which is to be formed upon filling of the crack. This approach can easily be implemented in a layout as shown in figure 2. If substrate and thin film properties are known, the crack termination point can be located with respect to the initiation point using a similar crack propagation study. For example, curved end-effectors of the microgripper in [18] were formed with this approach.

3. Crack–crack interactions

3.1. Experimental observations

Two sets of Si/SiO_2 samples with crack initiating triangular features were prepared using the procedure described in section 1. In the first set, an array of crack initiators were placed with a period of 50 μm along straight lines (figure 9(a)). In the second set this period was reduced to 20 μm (figure 9(b)). Both micrographs in figure 9 have the same magnification. It was observed that there was no crack–crack interaction in figure 9(a). Therefore, for this specific thin film–substrate system one can infer that the disturbance of the stress field by the presence of a crack does not extend over a distance of 50 μm. However, when this distance was reduced to 20 μm, cracks were observed to bend toward previously formed neighboring cracks and meet their traction-free faces perpendicularly. Considering that the oxide film thickness was 5 μm in this particular study, one can conclude that the interaction length was between 20 and 50 μm, i.e. 4–10 times the film thickness.

3.2. Computational modeling

To simulate the interaction between neighboring cracks, the geometry given in figure 3(b) was used where the distance between two interacting cracks, D, was varied from 4 and 8 to 10 times the film thickness, $h = 5$ μm [24]. The substrate thickness (400 μm) was 80 times the film thickness. The elastic mismatch between the thin film and the substrate varied to cover a wide range of material combinations. Similar to the cases studied for the crack-free edge interaction, three distinct values for α were considered: $\alpha = -0.36$, 0.36 and 0.79 with $\beta = \alpha/4$.

The finite element model for this problem includes 1.5 million degrees of freedom and a total of 500 000 tetrahedral and hexahedral elements for the elastic substrate and the thin film, respectively. The longer crack in the film was kept stationary whereas the shorter one was allowed to propagate. Any mode-mixity due to the neighboring long crack was expected to turn the shorter crack. Boundary conditions were kept the same as in the case of crack-free edge interactions and thermal body forces were introduced by imposing a temperature drop.

Resulting crack paths are plotted in figure 10. The following issues were evident on these plots:

- For $\alpha = -0.36$, interaction between cracks occurred only when D/h was reduced to 4 (figure 10(a)). In this case, the interaction between crack tip stress fields lead to an outward shift of the propagating crack indicating repulsion. No interaction was observed for $D/h = 8$ and $D/h = 10$ given in figures 10(b) and 10(c), respectively.
- For $\alpha = 0.36$, interaction occurred when $D/h = 4$ and 8. The propagating crack turned toward the existing crack for the $D/h = 4$ case (figure 10(a)). Compared to $\alpha = -0.36$, this turn took place earlier, indicating a stronger interaction. When the distance between cracks was increased to $D/h = 8$ (figure 10(b)), the crack

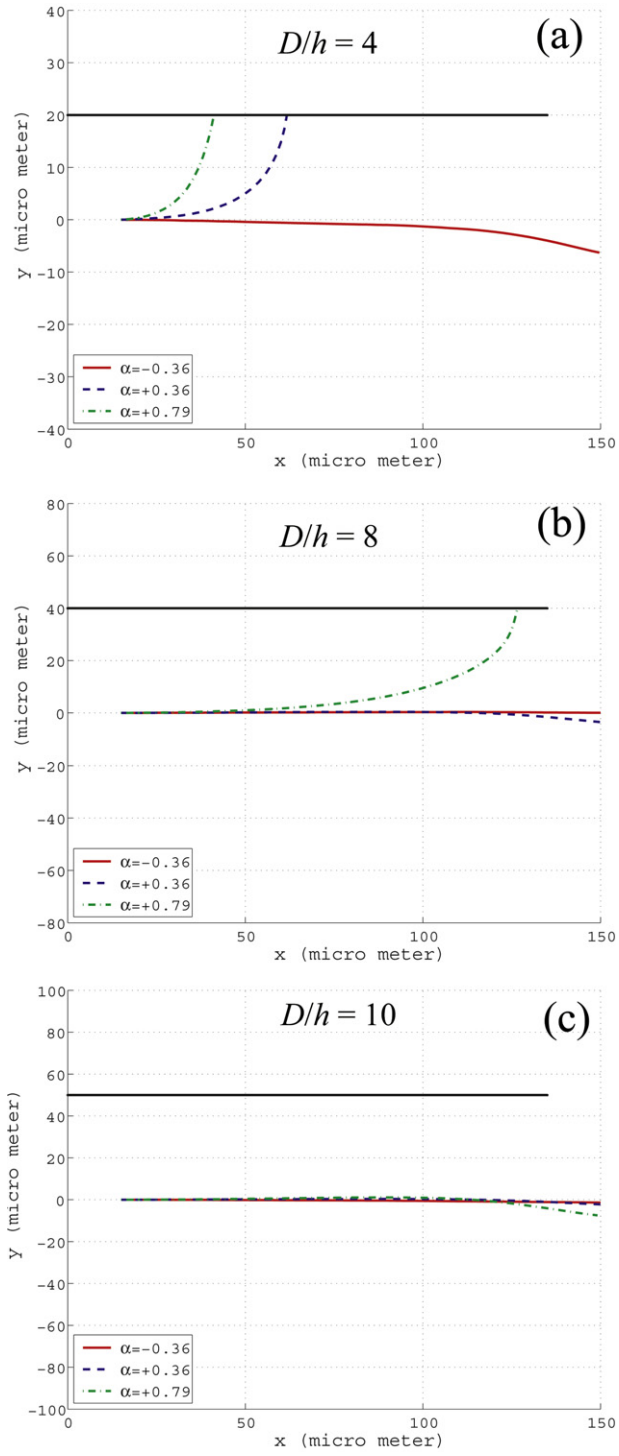

Figure 10. Crack–crack interactions with the same set of elastic mismatch as in figure 7. Crack spacing/film thickness ratio, D/h, is as follows: (a) $D/h = 4$, (b) $D/h = 8$, (c) $D/h = 10$.

retained its straight trajectory until it reached the vicinity of the tip of the neighboring long crack. At this point, the crack was observed to shift slightly outward, as was the case for the lower α at $D/h = 4$.

- Finally, when α was increased to 0.79, the cracks interacted for all cases considered. For $D/h = 4$ and 8 the propagating crack turned toward and met the existing crack at 90°. The amount of interaction decreased with increasing distance between the cracks as manifested by the reduced curvature in figure 10(b) compared to that of figure 10(a). The slight outward shift was also delayed until D/h was increased to 10.

For a discussion of these observations, one can refer to the interaction (or decay) length, l, introduced by Xia and Hutchinson [4]. l is a property of the thin film–substrate system and describes the extent of the neighborhood over which changes in the stress state transverse to an isolated, semi-infinite crack take place. The normal stress component transverse to the crack face will assume the value of zero at the crack face due to the traction-free boundary condition and will slowly increase and reach a far-field value as one moves away. The build-up of the transverse stress component obeys an exponential function with a characteristic length l. Hence, l serves as a measure of the size of the neighborhood of reduced stresses around a crack and is given by

$$l = \frac{\pi}{2} g(\alpha, \beta) h \tag{3}$$

where h is the film thickness and $g(\alpha, \beta)$ is a non-dimensional quantity describing the integral of the crack opening displacement with α and β as the two Dundurs' parameters [4]. The function is reported to exhibit a weak dependence on β [5]. l increases proportional to the film thickness. If there is no elastic mismatch, i.e. if $\alpha = \beta = 0$, l becomes almost twice the film thickness. If the film stiffness is much higher than that of the substrate, i.e. if α is large, l becomes larger than the film thickness thereby increasing the size of the region over which crack–crack interactions are expected to take place. However, with decreasing film stiffness, l will be reduced to the order of the film thickness.

In line with the previous observations given in figure 7, the amount of interaction in figure 10 increases with increasing α. To compare results with theory, the corresponding theoretical interaction length, l, for each case should be computed from equation (3). Computed values can then be used to explain the interactions of parallel cracks with the analysis of Xia and Hutchinson [4].

Let us first consider the mismatch of $\alpha = -0.36$. When $\alpha = -0.36$ and $\beta = \alpha/4$, the theoretical interaction length is at its minimum with $l = 1.6h$. In other words, the zone of reduced stresses has a smaller extent as compared to those with higher α values. As a result, cracks are to be more closely spaced for an interaction to occur. In fact, for the studied parallel crack configuration, Xia and Hutchinson's [4] solution predicts crack attraction at a crack spacing of $D/l = 2$, corresponding to $D/h = 3.2$ in our specific case. This value is smaller than all D/h values considered in this work. Hence, the lack of crack–crack interaction in finite element modeling with $\alpha = -0.36$ is in parallel with this theoretical prediction.

Similarly, the crack tip repelling phenomenon of figure 10(a) with $\alpha = -0.36$ matches well with the results of Xia and Hutchinson [4]. Two parallel cracks of the same length are predicted to repel each other if they are within $D/l = 4$ [4]. $D/l = 4$ corresponds to $D/h = 6.4$ in reference. Hence, no

repulsion is visible for $D/h = 8$ and 10 as opposed to the case of $D/h = 4$.

When α is increased to 0.36 with $\beta = \alpha/4$, the interaction length also increases to $l = 2.8h$ corresponding to a critical spacing of $D/h = 5.6$. This amount is lower than $8h$ (figure 10(b)) and $10h$ (figure 10(c)). Hence, the only interaction is again evident in figure 10(a), whereas a small repelling effect is observed in figure 10(b).

Finally, for $\alpha = 0.79$, the interaction length attains its maximum value of $l = 5.5h$. Using $D/l = 2$, the critical interaction spacing of $D/h = 11$ is obtained. Therefore cracks are observed to interact over a distance of $8h$ (figures 10(a) and (b)). When the distance between cracks is increased to $10h$ (figure 10(c)), some attraction is still evident in the form of a minute bending of the crack path. However, once the crack tips get closer, the repulsive effect becomes dominant.

4. Conclusions

In this work, a crack in a thin film was put into interaction either with a free edge or with a neighboring crack and the resulting propagation behavior was studied. The thin film–substrate system was simulated using finite element analysis. Depending on material properties of the thin film and the substrate, different crack propagation paths were observed. The following conclusions are reached as a result:

(i) Curved crack front model ensures constancy of energy release rate and increases the reliability of crack propagation simulations. It leads to a stronger interaction when compared to a straight crack front.

(ii) With increasing α, which corresponds to an increase in film stiffness, a higher level of interaction is observed. A stronger interaction is also evident with lower β for all α values studied. The level of this interaction sets the lower limit to the period of an array of straight NWs. With increasing interaction, dense packing of NWs becomes a challenge. For a relatively compliant thin film, such as SiO_2 on Si, packing period can be less than eight times the film thickness.

(iii) Simulations are ultimately needed to predict crack paths prior to placement of stress raisers and free edges on a substrate through etching. Once these entities are defined, a rational assembly of cracks takes place. This is, in principle, similar to dielectrophoretic or magnetic assembly, where an external field is utilized to align NWs based on their shape anisotropy. As opposed to many self-assembly processes, however, stress-guided crack formation can be carried out deterministically with very high precision. Achieving a single NW per contact is the usual practice. Although there is a limit on how close one can bring a pair of cracks together, the proposed fabrication approach is ideal for the integration of microsystems with NWs, where the precision of placement is more important than a high spatial density of NWs.

Acknowledgments

The experiments were performed at the Department of Mechanical Science and Engineering at the University of Illinois at Urbana-Champaign. Support from Professor H Sehitoglu and Professor T Saif is gratefully acknowledged. BEA acknowledges support by Tübitak under grant no. 104M216 and the TÜBA-GEBİP Distinguished Young Scientist Award. GA acknowledges partial support of State Planning Agency (DPT) through grant no. DPT 01 K 120270. Some of the simulations were performed at Ozen Engineering. We would like to thank Dr M Ozen and Dr D Wagner for their support.

References

[1] Hutchinson J W and Suo Z 1992 Mixed mode cracking in layered materials *Adv. Appl. Mech.* **29** 63–191

[2] Chen S-Y and Chen I-W 1995 Cracking during pyrolysis of oxide thin films—phenomenology, mechanisms, and mechanics *J. Am. Ceram. Soc.* **78** 2929–39

[3] Chow L A, Dunn B, Tu K N and Chiang C 2000 Mechanical properties of xerogel silica films derived from stress versus temperature and cracking experiments *J. Appl. Phys.* **87** 7788–92

[4] Xia Z C and Hutchinson J W 2000 Crack patterns in thin films *J. Mech. Phys. Solids* **48** 1107–31

[5] Beuth J L Jr 1992 Cracking of thin bonded films in residual tension *Int. J. Solids Struct.* **29** 1657–75

[6] Ye T, Suo Z and Evans A G 1992 Thin film cracking and the roles of substrate and interface *Int. J. Solids Struct.* **29** 2639–48

[7] Liu X H, Suo Z, Ma Q and Fujimoto H 2000 Developing design rules to avert cracking and debonding in integrated circuit structures *Eng. Fract. Mech.* **66** 387–402

[8] Liang J, Huang R, Prévost J H and Suo Z 2003 Evolving crack patterns in thin films with the extended finite element method *Int. J. Solids Struct.* **40** 2343–54

[9] Salac D and Lu W 2006 Controlled nanocrack patterns for nanowires *J. Comp. Theor. Nanosci.* **3** 263–8

[10] Alaca B E, Sehitoglu H and Saif T 2004 Guided self-assembly of metallic nanowires and channels *Appl. Phys. Lett.* **84** 4669–71

[11] Thurn J and Cook R F 2002 Stress hysteresis during thermal cycling of plasma-enhanced chemical vapor deposited silicon oxide films *J. Appl. Phys.* **91** 1988–92

[12] Mani S and Saif T M 2005 Mechanism of controlled crack formation in thin-film dielectrics *Appl. Phys. Lett.* **86** 201903

[13] Mani S and Saif T M 2007 Stress development in plasma-deposited silicon dioxide thin-films due to hydrogen evolution *Thin Solid Films* **515** 3120–5

[14] Sardan O, Yalcinkaya A D and Alaca B E 2006 Self-assembly-based batch fabrication of nickel–iron nanowires by electroplating *Nanotechnology* **17** 2227–33

[15] Adelung R, Aktas O C, Franc J, Biswas A, Kunz R, Elbahri M, Kanzow J, Schurmann U and Faupel F 2004 Strain-controlled growth of nanowires within thin-film cracks *Nat. Mater.* **3** 375–9

[16] Elbahri M, Rudra S K, Wille S, Jebril S, Scharnberg M, Paretkar D, Kunz R, Rui H, Biswas A and Adelung R 2006 Employing thin-film delamination for the formation of shadow masks for nanostructure fabrication *Adv. Mater.* **18** 1059–62

[17] Jebril S *et al* 2008 Integration of thin-film-fracture-based nanowires into microchip fabrication *Small* **4** 2214–21

[18] Sardan O, Alaca B E, Yalcinkaya A D, Bøggild P, Tang P T and Hansen O 2007 Microgrippers: a case study for batch-compatible integration of MEMS with nanostructures *Nanotechnology* **18** 375501
[19] Thouless M D 1990 Crack spacing in brittle films on elastic substrates *J. Am. Ceram. Soc.* **73** 2144–6
[20] Yin H M, Paulino G H and Buttlar W G 2008 An explicit elastic solution for a brittle film with periodic cracks *Int. J. Fract.* **153** 39–52
[21] Huang R, Prévost J H, Huang Z Y and Suo Z 2003 Channel-cracking of thin films with the extended finite element method *Eng. Fract. Mech.* **70** 2513–26
[22] Liu L and Chen X 2008 Controlled crack arrest in brittle thin films: the effect of embedded voids *Acta. Mater.* **56** 6214–23
[23] Erdogan F and Sih G C 1963 On the crack extension in plates under plane loading and transverse shear *J. Basic Eng.* **85** 519–27
[24] Ozcan C 2006 The effect of interface strength on crack interactions in thin film coated substrates *MS Thesis* Boğaziçi University Istanbul, Turkey.
[25] Dundurs J W 1969 Edge-bonded dissimilar orthogonal elastic wedges *J. Appl. Mech.* **36** 650–2
[26] Brantley W A 1973 Calculated elastic constants for stress problems associated with semiconductor devices *J. Appl. Phys.* **44** 534–5
[27] Cao Z, Zhang T-Y and Zhang X 2005 Microbridge testing of plasma-enhanced chemical-vapor deposited silicon oxide films on silicon wafers *J. Appl. Phys.* **97** 104909
[28] Shen Y-L, Suresh S and Blech I A 1996 Stresses, curvatures, and shape changes arising from patterned lines on silicon wafers *J. Appl. Phys.* **80** 1388–98
[29] Nakamura T and Kamath S M 1992 Three-dimensional effects in thin films *Mech. Mater.* **13** 67–77